RSC Advances

PAPER

View Article Online
View Journal | View Issue

Cite this: *RSC Adv.*, 2018, **8**, 35651

Extracellular pH imaging of a plant leaf with a polyelectrolyte multilayered nanosheet†

Daichi Someya,[a] Satoshi Arai,[bc] Toshinori Fujie *[de] and Shinji Takeoka *[a]

Received 26th July 2018
Accepted 7th October 2018

DOI: 10.1039/c8ra06308g

rsc.li/rsc-advances

We have developed a sheet-like pH imaging sensor based on a flexible and physically adhesive polymer thin film (referred to as a "pH sensing nanosheet"). The pH sensing nanosheet was composed of two films: one is a pH-sensitive layer-by-layer (LbL) film constructed from fluorescein-conjugated poly(acrylic acid) and poly(allylamine hydrochloride) and the other is a pH-insensitive film made from Nile red-embedded poly(D,L-lactic acid). The pH sensing nanosheet enabled the ratiometric imaging of pH changes in a leaf (500 × 500 μm^2), namely the apoplastic ion milieu responding to an external NaCl stress. It was successfully mapped out that the alkalization of the leaf apoplast spread from the leaf base to the tip at 20 min after the stimulation and the pH value increased up to approximately pH 6.3 from less than pH 4.5 within 60 min when a 100 mM NaCl aqueous solution was added. The pH sensing nanosheet should be useful for energy metabolic mapping in tissue biology.

Introduction

An understanding of the spatial dynamics of cellular signaling molecules such as Ca^{2+}, cAMP, and reactive oxygen species is essential over a wide-range of biological research.[1–3] Furthermore, enormous efforts have been dedicated to comprehend how physicochemical parameters such as temperature, viscosity, and pH are altered during biological events.[4,5] Among them, pH is a very common parameter that garners attentions because it changes in relation to the changes in energy metabolisms[6] and immune responses caused by physical or chemical stresses.

To map out the spatial information of pH with high resolution, optical sensors using fluorescent signals are most common tools.[7] To date, various optical sensors have been developed, which include fluorescent protein-based indicators (*e.g.* pHluorin and pHRed)[8] and small chemical dyes (*e.g.* SNARF series).[9] Though it is quite obvious that fluorescent protein-based sensors have benefited recent biological studies, this method, which uses a genetically encoding technique, requires troublesome procedures to produce a wide variety of transgenic animals or plants. On the other hand, fluorescent dye-based pH sensors are easy to handle and are accessible to researchers who are not familiar with genetic engineering. However, in the case of *in vivo* imaging, it is difficult for those probes to be loaded properly in biological tissues and to be observed accurately. For example, it is unclear how deep the fluorescent dye penetrates from a tissue surface and whether its distribution is uniform or not.[10]

While current imaging studies mainly focus on the intracellular pH, the demand to image the pH of extracellular environments is growing. Therefore, small chemical dyes are used that are conjugated with water-soluble polymers to prevent cell internalization.[11] Alternatively, the other approach employed nanoparticles embedding pH-sensitive dyes that can be accumulated onto the tissue surface.[12] Furthermore, Ke *et al.* reported a more sophisticated way whereby an amphiphilic lipid-DNA molecule used for cell-membrane penetration is covalently modified with pH indicators.[13] However these approaches do not fully meet the requirements for a robust fluorescent pH sensor under extracellular conditions. For instance, "perfect immobilization" of pH sensors to the plasma membrane may be impossible which means that sensory materials are partially located in intracellular spaces due to endocytosis and lipid flip-flop or are distributed throughout an entire tissue and in blood and are washed out quickly.[14]

Herein, we propose a thin film-type fluorescent sensor, named "pH sensing nanosheet" that can directly attach onto tissue surfaces and provide distinct pH mapping images. So far, the reported sheet-like pH sensory materials are optically transparent polymeric matrices such as poly(2-hydroxyethyl methacrylate),[15] polyurethane hydrogel,[16] and tetraethyl orthosilicate (TEOS) based sol–gel films[17] coupling with a variety of

[a]*Department of Life Science and Medical Bioscience, Waseda University, TWIns, 2-2 Wakamatsu-cho, Shinjuku-ku, Tokyo 162-8480, Japan. E-mail: takeoka@waseda.jp*
[b]*PRIME, Japan Agency for Medical Research and Development (AMED), Tokyo 100-0004, Japan*
[c]*Research Institute for Science and Engineering, Waseda, University, Japan*
[d]*Waseda Institute for Advanced Study, Waseda University, TWIns, 2-2 Wakamatsu-cho, Shinjuku-ku, Tokyo 162-8480, Japan. E-mail: t.fujie@aoni.waseda.jp*
[e]*Japan Science and Technology Agency, PRESTO, 4-1-8 Honcho, Kawaguchi, Saitama 332-0012, Japan*

† Electronic supplementary information (ESI) available. See DOI: 10.1039/c8ra06308g

pH indicators.[18] Though these materials have sufficient proton-permeability and biocompatibility for a pH sensor, their usability is limited due to their thickness and low flexibility. Schreml *et al.* reported a luminescence sensor film for high-resolution pH imaging to analyze disease processes, such as wound healing and tumor metabolism.[19] The sensor film had poor adhesion and the inclusion of air bubbles underneath the films occurred due to its thickness, which was approximately 6 μm.

Our group has engineered nanosheets, of which are only tens or hundreds of nm in thickness, and which possess several features such as a free-standing structure, high flexibility and adhesiveness to uneven surfaces without the use of any glue.[20] In a recent study, temperature mapping with high spatial resolution has been achieved with luminescence nanosheets having thermo-sensitive and insensitive dyes.[21] Likewise, the pH sensing nanosheet was designed to comprise both pH sensitive and insensitive films. The combination of two films allows ratiometric analysis to circumvent common obstacles such as focus drift or variation of excitation light intensity. Furthermore, by employing a layer-by-layer (LbL) method,[22] we were able to make a thinner and ion-permeable sensor film and a pH-insensitive film that served as a physical support for a ratiometric measurement. LbL engineered thinner film is suitable for plant imaging because plant tissues have heterogeneous surfaces such as much-branched roots and leaves with fine texture, on which it is difficult for conventional rigid pH sensing films to attach.

As a result, we have demonstrated extracellular pH imaging in plant tissues in which the ionic gradients are directly affected by a growth factor (auxin; indole-3-acetic acid) stimulus[23] or stressful environments (*e.g.* drought or salinity).[24] It has been reported that NaCl stress activates a defense system of plants to prevent excess uptake of Na^+ and Cl^- ions involving alkalization of the external (apoplastic) pH, stomatal closure and reduction of the transpiration rate.[25] In this paper, we use our system to image the extracellular pH dynamics of apoplastic ion milieu induced by salt stress in *Lilium longiflorum*.

Results and discussion

Material design

For the ratiometric pH imaging, a pH-sensitive hydrophilic dye – fluorescein – and a pH-insensitive lipophilic dye – Nile red – were employed. Fluorescein is known to have a high quantum yield and a pH-dependent fluorescence property, which are suitable for pH measurements. The pH sensitivity is mainly attributed to the deprotonation of the hydroxy group of the xanthene ring(Fig. S1†), whose pK_a value is approximately 6.7.[26] The fluorescein molecule should be immobilized in proton-permeable polymer matrices since the hydrophilic dye is subject to leaching from the sensor film. Therefore, we covalently conjugate an amino derivative of fluorescein (fluoresceinamine isomer I) to the carboxylic group of PAA by an amide linkage (Fig. S2†). Then, the resulting fluorescein-labelled PAA is incorporated into the polyelectrolyte multilayer film during LbL processing, followed by crosslinking. On the other hand, hydrophobic Nile red is non-covalently incorporated into the PDLLA film by mixing it with a PDLLA solution in a spin-coating process. Finally, the fluorescein-conjugated LbL film and the Nile red-embedded PDLLA film are physically overlaid to form a free-standing pH sensing nanosheet.

Preparation and characterization of pH sensing nanosheet

The Nile red-embedded PDLLA film that serves as a pH-insensitive film was spin-coated on the surface of a PVA-pre-coated SiO_2 substrate, where the water-soluble PVA layer was used for exfoliation of the film (thickness: 118 ± 4 nm) (Fig. S3†). In addition, the polyelectrolyte multilayer film composed of PAH and PAA, was prepared on the surface of the Nile red-embedded PDLLA film by the LbL method, resulting in a thickness of 35 ± 7 nm with 5 layer pairs. Next, the 93 ± 4 nm thick pH-sensitive film (30 layer pairs) was spincoated (Fig. 1a).

The thickness was proportional to the number of layer pairs, even after changing the PAA layer to the fluorescein-conjugated PAA layer (introduced from the 6th layer pair onwards). The thickness of single PAH/PAA bilayer (approximately 3.9 nm) (Fig. 1b) agrees with the previous report.[27] The resulting LbL film was hydrophilic, which was confirmed by a contact angle measurement (Fig. S4†). As the number of layer pairs was raised, the contact angle significantly decreased. It was reported

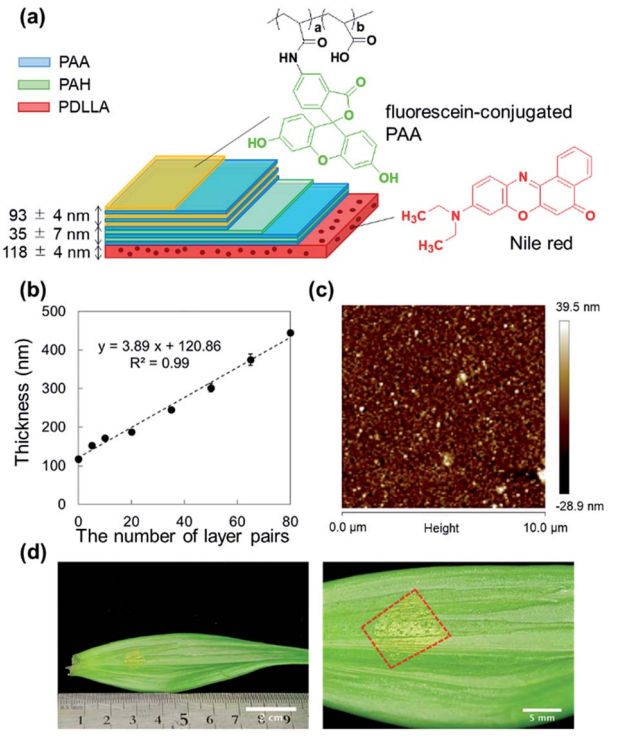

Fig. 1 (a) Structure of a pH sensing nanosheet composed of PAA/PAH multilayer (35 pairs) film with fluorescein-conjugated PAA film (30 pairs) and Nile red-embedded PDLLA supporting film. (b) Thickness of the pH sensing nanosheet as a function of the number of layers. (c) AFM surface morphology of the pH sensing nanosheet. (d) Microscopic image of a pH sensing nanosheet attached to an adaxial leaf surface. *i.e.*, the upper epidermis was partially removed by tweezers for pH analysis.

that a PAH/PAA bilayer exhibited wettable surfaces ($18 \pm 5°$).[28] It is reasonable that contact angles of fluorescein-incorporated PAH/PAA bilayer were $28 \pm 0°$. Next, the pH sensing nanosheet composed of a pH-sensitive LbL film and a pH-insensitive PDLLA film was then thermally crosslinked at 100 °C to enhance its physical stability. The thermal crosslinking of the LbL layer was confirmed from the decrease in the peak intensity at 1580 cm^{-1}, which is attributed to the amine group of PAH, using FT/IR spectroscopy (Fig. S5†). It was reported that PAA/PAH LbL assemblies underwent curing *via* anhydride formation and amidation upon heating[29] so that the LbL films need to be cured above 100 °C to accelerate the crosslinking. However, the sacrificial layer method would not work when exposed at severe high-temperature conditions (above T_g of polyvinyl alcohol; 85 °C) for long time. In fact, the nanosheet could not be peeled off and was broken into pieces when placed in an oven at 120 °C (data not shown). Hence, we used the heating conditions of 100 °C and 5 hours to confirm the increment of the contact angle (Fig. S4†). After thermal crosslinking, the nanosheet was immersed in a pH 9.0 Britton–Robinson (B–R) buffer for 24 hours to wash out unfixed fluorescein-conjugated PAA. The final pH sensing nanosheet obtained by dissolving the PVA layer showed a smooth surface and good adhesion to the surface of *Lilium longiflorum* leaf (Fig. 1c and d), on which no cracks or air bubbles appeared thanks to its high flexibility.

Spectral properties

The fluorescein-conjugated LbL film and the Nile red-embedded PDLLA film were fabricated individually. The fluorescence spectrum of each dye meets the standards of FITC (475/530 nm) and TRITC (542/620 nm) filters, respectively (Fig. 2a, d). The fluorescein-conjugated LbL film ($\lambda_{ex} = 493$ nm, $\lambda_{em} = 520$ nm) exhibited a pH sensitivity similar to fluorescein dissolved in an aqueous solution (Fig. 2b). The fluorescence intensity of fluorescein obeyed a sigmoidal curve and could be fitted by a Boltzmann function according to eqn (1).

$$I = \frac{m_1 - m_2}{1 + \exp\left(\frac{pH - pK_a}{p}\right)} + m_2 \quad (1)$$

where the I values are normalized fluorescence intensities measured at varying pH values. The parameters: m_1, m_2, pK_a, and p are empirical parameters describing the initial value, the final value, the point of inflection, and the width of the sigmoidal curve, respectively. From the peak intensity plotted with respect to pH, the calculated pK_a value was 6.83 which is good agreement with that of fluorescein[26] (Fig. 2e). On the other hand, the Nile red-embedded PDLLA film ($\lambda_{ex} = 548$ nm, $\lambda_{em} = 582$ nm) was unaffected by the pH of the aqueous solution (Fig. 2d). The fluorescence intensities of Nile red were almost constant *versus* pH change (0.12% pH^{-1}, relative to pH 4.5) (Fig. 2f).

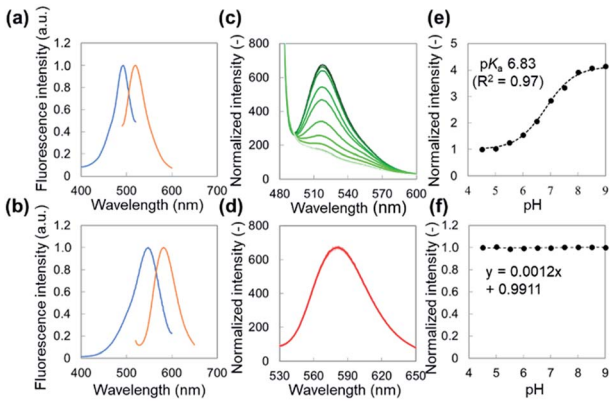

Fig. 2 Fluorescence properties of pH sensitive and insensitive films: excitation and emission spectra of (a) fluorescein-conjugated LbL film, (b) Nile red-embedded PDLLA film. Emission spectra of (c) fluorescein-conjugated LbL film, (d) Nile red-embedded PDLLA films when pH was raised from 4.5 to 9.0 (every 0.5). Normalized peak intensities of (e) fluorescein-conjugated LbL film and (f) Nile red-embedded PDLLA film were plotted against pHs (normalized at pH 4.5). Boltzmann fitting was chosen for fitting the sigmoidal curves.

Evaluation of dye leaking, reversibility, and response time

In order to monitor pH dynamics on wet surfaces, the pH sensing nanosheet should prevent the leakage of the dyes in physiological environments. In this regard, as unfixed fluorescein-conjugated PAA had been washed out by immersing in a pH 9.0 of Britton–Robinson (B–R) buffer for 24 hours in advance (Fig. S6a†), the leakage of fixed fluorescein was not detected by spectrophotometry even when the nanosheet was exposed to PBS (pH 7.4) for 24 hours on a shaker (37 °C, 50 rpm) (Fig. S6b†). Then, the fluorescence intensity was reversibly shifted at least four cycles between acidic (pH 5.0) and basic (pH 9.0) of B–R buffers without decomposition and was stable against photobleaching for 10 min (Fig. S7†). The pH sensing nanosheet was judged to be ready for applications involving drastic pH changes such as acute wound healing and long-term pH monitoring using time-lapse imaging.

The response time of the sheet was defined as the time taken for the signal to achieve 90% of the equilibrium state, as stated in the literature.[30] The response time was measured to be less than 20 s (Fig. S8†), which was at least three times faster than those reported previously.[31,32] The response time was mainly dependent on the matrix thickness (0.12 nm s^{-1}). It is thought that the response time differs according to the proton permeability of the polymer matrices. Generally, the thicker sensing films need more time to sense the proton concentration of buffer solutions. On the other hand, thinner sensing films, thus containing a lesser amount of indicator, result in a lower fluorescence intensity, which sometimes cannot be distinguished from autofluorescence. Therefore, the fluorescence intensity was increased by increasing the number of fluorescein-conjugated PAA layers to overcome the autofluorescence from tissue.

pH calibration on leaf surfaces

Autofluorescence is a major obstacle to obtain a mapped image of the pH distribution. However, as shown in Fig. 3a–d, autofluorescence of the plant tissues was weak enough that it was

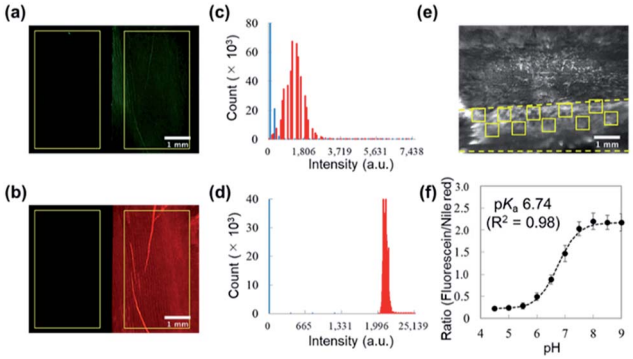

Fig. 3 Fluorescence properties of the pH sensing nanosheet on adaxial leaf surfaces: microscopic images of (a) fluorescein observed by a GFP channel and (b) Nile red observed by an RPF channel (scale bar: 1 mm). Region of interests (ROI; 2.5 × 4.5 mm^2) were chosen from the tissue-peeled area and nanosheet-attached area, respectively. Histogram of fluorescence intensity of (c) fluorescein and (d) Nile red compared with autofluorescence from the palisade tissue (blue: autofluorescence, red: nanosheet). (e) Ratiometric fluorescence image of the pH sensing nanosheet immersed in a B–R buffer at pH 9.0 (scale bar: 1 mm). Region of interests (ROI; 500 × 500 μm^2) were chosen at 10 spots from the peeling area (between dashed lines). (f) Ratiometric fluorescence intensity of the nanosheet plotted against pH 4.5–9.0 (normalized at pH 4.5). The calibration curve allowed to calculate the pH value by solving a Boltzmann fit equation.

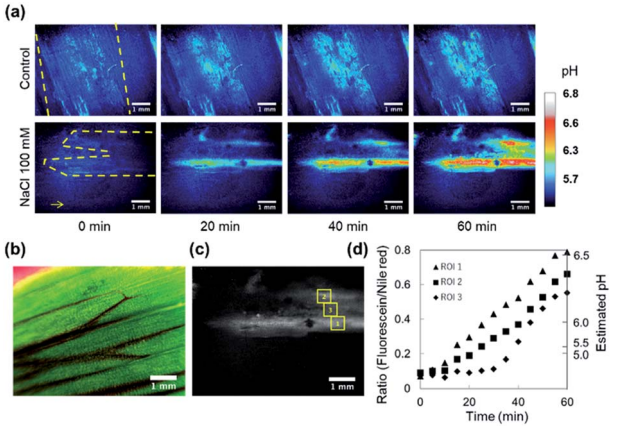

Fig. 4 Ratiometric pH imaging of adaxial leaf apoplast under 100 mM NaCl stress: (a) pseudo color maps obtained by fluorescent ratio images of the pH sensing nanosheet (scale bar: 1 mm). Color is corresponding to the normalized ratio intensity. pH values with a color scale was calculated from a calibration curve. The arrow represents the direction to the tip of leaf. (b) Bright field image of the leaf surface after epidermal peeling stained with rhodamine B (scale bar: 1 mm). (c) Fluorescent ratio image of the pH sensing nanosheet attached to the leaf suffering salinity stress for 60 min (scale bar: 1 mm). Region of interests (ROI; 500 × 500 μm^2) were chosen at 3 spots at right angle to vascular bundles within the peeling area. (d) The pH dependence of normalized ratio intensities within each ROI. The pHs were estimated by calibration data.

negligible for determining accurate pH values. For converting the fluorescence ratios into pH values, we performed a pH calibration using the nanosheet adhered on adaxial leaf surfaces. The pH calibration curve was acquired by dropping pH-adjusted B–R buffers onto the nanosheet (Fig. 3e). The pH-dependent fluorescence intensity at the region of interest (ROI) showed a sigmoidal curve, and the pK_a value (6.74) was similar to that was measured with the spectrophotometer (Fig. 3f).

The pH resolution was calculated by dividing the standard deviation of fluorescence intensity by the slope of the sigmoidal curve at each pH value. The sigmoidal curve exhibits a slope around the pK_a value so that the pH sensing nanosheet would show the highest pH sensitivity around pH 6.7. According to this result, the pH resolution was approximately 0.2 in the range of pH 5.5–7.0. Then we calculated the spatial resolution which was defined as the pH resolution at each ROI size. As shown in Fig. S9,† the pH resolution dropped at a smaller ROI. It is concluded that pH can be estimated to have an error of 0.2 over at least 300 × 300 μm^2.

Ratiometric pH imaging of the plant leaf

It is known that the apoplastic pH of leaves is alkalized in respond to NaCl stress. As the Cl^- concentration in the apoplast is increased, the Cl^- uptake from the apoplast into cells energetically coupled to the symport of protons is promoted.[33] The reflux of protons induces the apoplast alkalization and subsequently leads to the reduction of the transpiration rate. This phenomenon is thought to be a defense mechanism against soil salinity.[34]

In this regard, we evaluated the dynamics of apoplastic pH on adaxial leaf surfaces. The apoplastic pH was successfully mapped out with the pH sensing nanosheet. The pH value at the peeled area increased up to approximately pH 6.3 from less than pH 4.5 within 60 min when a 100 mM NaCl aqueous solution was added from petiole, while D. I. water (control) did not induce the alkalization. In addition, it can be seen from the ratio image at 20 min after the stimulation that the alkalization of the leaf apoplast spread from the leaf base to the tip (Fig. 4a). These results are in good agreement with a previous report by Geilfus *et al.*[35] The width of veins was approximately measured to be 1.0 mm by a bright field image (Fig. 4b). Then, the fluorescence intensities were analyzed at 3 ROIs located on the vertical direction of veins of the leaf (Fig. 4c and d). These results suggested that the apoplast alkalization heterogeneously occurred from the veins, which was consistent with previous studies.[36]

In future, our pH sensing nanosheet needs to be effective over long term pH monitoring in tissue than hours (*e.g.*, a few days). This is important because our group has already demonstrated that LbL nanosheet for treatment of gastrointestinal tissue defects exhibited no tissue adhesion for a week[37] and confirmed that the presence of PDLLA nanosheet does not affect the cytotoxicity.[38] Although some polyelectrolytes may be cytotoxic, it was reported that incorporation of PAA and PAH polyelectrolytes into LbL multilayers neutralized the cytotoxic effects through the stable polyvalent polyanion–polycation interactions that inhibit the membrane destruction forces and possible internalization of toxic amounts of polyelectrolyte by endocytosis.[39] By its virtue of the perfect immobilization of pH sensory materials, it enables the end-users of our pH sensing nanosheet to be convinced that

the pH can be definitely monitored on "the surface" of biological samples. We expect that our pH sensing nanosheet will contribute not only to basic research in plant biology but also to biomedical research in wound healing and cancer treatments.[40]

Conclusions

We have developed a free-standing pH sensing nanosheet based on a ratiometric method that enables sub-micrometer dimension mapping with a fluorescence stereo microscope. The pH sensing nanosheet exhibited good reversibility, high photostability, and a short response time for the real-time pH mapping. We demonstrated a heterogeneous pH distribution within apoplasts in response to salinity stress by attachment of the nanosheet on the plant leaf. The pH sensing nanosheet will be useful not only for plant research about resistance to salt stress, but also for biomedical research by adjusting the fluorescence intensity (optimizing the sensor thickness) to overcome autofluorescence from animal tissues. The present sensing system based on LbL assembly can provide a variety of sensing nanosheets using other analytical parameters by changing the indicator dyes. Such multiple combinations of sensor nanosheets should enable the consistent analysis of metabolism, signaling, and the immune system from cells to tissues and bodies.

Experimental

Materials

Poly(acrylic acid) (PAA) (M_w: 300 000), *N*,*N*′-dicyclohexylcarbodiimide (DCC), and Nile red were purchased from Wako Pure Chemical Industries (Tokyo, Japan). Poly(vinyl alcohol) (PVA) (M_w: 22 000) and methanol-d4 for NMR were purchased from Kanto Chemical Industry (Tokyo, Japan). Poly(allylamine hydrochloride) (PAH) (M_w: 58 000), fluoresceinamine isomer I or 5-aminofluorescein, and Dulbecco's phosphate buffered saline (DPBS) were purchased from Sigma-Aldrich (St. Louis, MO). Poly(D,L-lactic) acid (PDLLA) (M_w: 600 000) was purchased from Polysciences, Inc. Spectra/Por 4 Membrane (MWCO: 12 000) for dialysis was purchased from Spectrum laboratories, Inc. Britton–Robinson (B–R) buffers composed of acetic acid, boric acid, phosphoric acid, and sodium hydroxide were used for tuning pH values. The pH values were determined with a digital pH meter F-51, HORIBA, Ltd. (Kyoto, Japan) calibrated with standard buffers of pH 4.0, 7.0, and 9.0. For fluorescence measurements, quartz glass plates purchased from Matsunami Glass Ind., Ltd. (Tokyo, Japan) were cut into a proper size (22 × 13.5 mm^2) using diamond files. Silicon wafers (SiO_2 substrate) purchased from KST World Co. (Fukui, Japan) cut into a proper size (typically 2 × 2 cm^2) were immersed in a mixture of sulfuric acid/hydrogen peroxide (3 : 1) for a 10 min wash and were then thoroughly rinsed with deionized (D.I.) water. A CaF_2 substrate for FT-IR analysis was purchased from Sigma-Koki Co., Ltd. (Tokyo, Japan). All organic solvents were purchased from Wako Pure Chemical Industries (Tokyo, Japan).

Synthesis of fluorescein-conjugated PAA

PAA (0.2 g, 2.78 mmol) and fluoresceinamine isomer I (193 mg, 0.56 mmol) were dissolved in 30 mL anhydrous DMF. The reactant solution was stirred for 30 min and put in an ice bath to decrease the temperature to 0 °C. DCC (172 mg, 0.83 mmol) dissolved in 10 mL dichloromethane was added to the solution. After stirring the reactant solution for 2 hours, we raised the temperature to room temperature and let the solution stand for another 3 days to complete the reaction. By-products were then removed with a paper filter. The sample was purified by dialysis (MWCO 12–14 000) in methanol, and the solvent was changed several times (200 mL of solvent, minimal 2 days of dialysis) until fluoresceinamine was not detected in the dialysate by spectrophotometer. The solvent was removed by a rotary evaporator and replaced with D.I. water. Then the compound was completely dehydrated using a freeze dryer. The purified polymers were characterized by ^{1}H-NMR (INOVA 400WB, Varian) (Fig. S10†). The conjugation rate ($a/a + b$) was estimated approximately 0.22, where a and b indicate the number of repeating units of fluorescein and acrylic acid, respectively.

Preparation of pH sensing nanosheet

The pH sensing nanosheet was composed of a Nile red-embedded PDLLA film and a fluorescein-conjugated LbL film. Those films were fabricated using a spin-coater (Opticoat MS-A150, Mikasa Co. Ltd., Tokyo, Japan) at 4500 rpm for 20 s. For fabricating the Nile red-embedded PDLLA film, PVA (2.0 wt%) was precoated on a SiO_2 substrate as a sacrificial layer. Nile red (0.001 wt%) and PDLLA (2.0 wt%) were dissolved in 10 mL of ethyl acetate. Then 0.5 mL of the solution was added onto the PVA layer and spin-coated to fabricate the Nile red-embedded PDLLA film. For fabricating the fluorescein-conjugated LbL film, PAA (0.1 wt%) and PAH (0.1 wt%) were dissolved in 100 mL of D.I. water, respectively. The PAH solution was spin-coated on the PDLLA-supporting layer. After spin-coating, the substrate was rinsed with D.I. water by spinning. Subsequently, the LbL procedure for each polyelectrolyte and water-rinse was alternately performed until 5 layer pairs (PAA stage) were generated. For making the films with 6 or more layer pairs, PAA was changed to the fluorescein-conjugated PAA (0.1 wt%). After spin-coating the fluorescein-conjugated film up to 35 layer pairs, the nanosheet was placed in an oven at 100 °C for 5 hours for crosslinking to occur between the amine groups of PAH and carboxyl groups of PAA. The crosslinking step of the LbL film was performed together with the underlying PDLLA layer and sacrificial PVA layer, and characterized by FT/IR-410 (JASCO Co., Tokyo, Japan). Samples for FT/IR were prepared by attaching the nanosheet on a CaF_2 substrate. The resulting film was immersed into a B–R buffer (pH 9.0) for 24 hours for washing out the fluorescein-conjugated PAA, which was not fixed on the nanosheet. Subsequently, a free-standing pH sensing nanosheet was obtained by immersing the substrate and film in D.I. water and dissolving the PVA layer. To attach the nanosheet onto a plant tissue surface, the nanosheet was scooped with a nylon mesh (SEFAR NYTAL HC-58, Sefer Co., Ltd.,

Switzerland). For the experiments of separate spectral properties, a Nile red-embedded PDLLA film and a fluorescein-conjugated LbL film were fabricated individually. LbL films were spin-coated up to 25 layer pairs on a PDLLA film without Nile red.

Characterization

The thickness of a fabricated nanosheet was evaluated with a Dektak XT-S stylus profiler (Bruker Corp., MA/USA). Its roughness was analyzed by atomic force microscopy (VN-8000, KEYENCE, Japan). The contact angles were collected 30 s after dropping (4 μL) and were calculated by a half-angle method. The measurements were performed under 22 °C, 42% humidity.

All spectral properties of the dyes incorporated in the fabricated nanosheet were analyzed with a spectrophotometer (RF-5300PC, SHIMAZU, Japan). The nanosheet was attached on a glass plate and fixed into a glass cuvette at an angle of 45°. The pH sensitivity was also obtained for the fabricated nanosheet by immersing it in several 3 mL B–R buffers adjusted to pH 4.5–9.0 (steps of 0.5 pH units). The sensitivity was calculated by plotting the peak fluorescence intensity of each spectrum. The peak intensity was normalized by the intensity of that at pH 4.5. Boltzmann fitting was chosen for fitting a sigmoidal curve to the pH sensitivity data. Fitting was performed by using the solver add-in in Excel.

For evaluating dye leaching, a set of nanosheets placed in 6-well plates were immersed in several 3 mL solutions of PBS (pH 7.4) on a shaker (BR-13UM, TAITEC) at 37 °C, 50 rpm. The fluorescence intensity of the collected solutions was measured by the spectrophotometer, and the amount of dye leakage was calculated from the calibration curve.

Sensor reversibility was confirmed by immersing a film in an acidic solution (pH 5.0) and a basic solution (pH 9.0), repeatedly. For examining photostability, the peak intensity was recorded for the neutral solution (pH 7.0) at after 10 min exposure at the maximum excitation wavelength. Finally, the response time was measured by titrating the pH of B–R buffers in a glass cuvette and by monitoring the fluorescence intensity. The pH of the buffer solution was adjusted using 2 M sodium hydroxide or hydrochloric acid and stirred with a multi-stir (CC-301, SCINICS).

Attachment of pH sensing nanosheet onto leaves

Lilium longiflorum was used as a model plant for the experiment investigating apoplastic pH imaging in response to NaCl stress. The lengths of long axis and short axis of the leaf were approximately 17 cm and 3 cm, respectively. The upper epidermis was carefully removed using with tweezers. The pH sensing nanosheet was cut to an optimal size using regular scissors (for pH imaging of plant leaves, approximately 10 × 10 mm^2). Then, the nanosheet was placed onto the peeled area of the adaxial leaf side, as the side of the LbL layers directly adhered on the surfaces (in case of pH calibration, the reverse side of the sheet was adhered). Changes in the apoplastic pH was induced by feeding the plant a 100 mM NaCl aqueous solution.

Ratiometric pH imaging

A fluorescence stereo microscope (MVX10 Macro Zoom System Microscope, Olympus, Tokyo, Japan) was used for fluorescence imaging experiments. For image capture, a CCD camera (DP72, Olympus, Tokyo, Japan) was used. A GFP filter (ISO 800, 1 s) for fluorescein and an RFP filter (ISO 200, 100 ms) for Nile red were used to observe the luminescence emission of the pH sensing nanosheet. The size of the observation field was 6.50 × 4.89 mm^2 covering 1360 × 1024 pixels. The ImageJ program was applied for the analyses of obtained images. Fluorescence ratio analysis provides correct quantitative fluorescence imaging with regard to artifacts in excitation light intensity and specimen shifts out of the focal plane, and photobleaching. Ratio (fluorescein/Nile red) images were obtained with the image calculator of ImageJ. For converting the fluorescence ratio data taken from living plants to apoplastic pH values, a calibration procedure was performed. A set of 20 μL B–R buffer (pH 4.5–9.0) solutions was applied to the adhered nanosheet and the ratio of the mean intensity for user-defined regions of interest (ROI; 500 × 500 μm^2) was calculated. Boltzmann fitting was chosen for fitting sigmoidal curves to calibration data. Time series were collected with a time interval of 5 min. For pseudo-color display, the ratio was coded by hue on a spectral color scale ranging from over blue (lowest ratio value; 0.00) to white (highest ratio value; 1.28), corresponding with the calibration data.

Conflicts of interest

There are no conflicts to declare.

Acknowledgements

This work was supported by JSPS KAKENHI: Grant Number 16K14009, 18H03539, 18H05469 and 17K20116, the Precursory Research for Embryonic Science and Technology (PRESTO) from the Japan Science and Technology Agency (JST; grant number JPMJPR152A), the Noguchi Institute, and the Tanaka Kikinzoku Memorial Foundation. The authors appreciated Mr Isao Takahashi for the preparation of LbL films.

References

1 J. T. Russell, *Br. J. Pharmacol.*, 2011, **163**, 1605–1625.
2 H. Kasai and O. H. Petersen, *Trends Neurosci.*, 1994, **17**, 95–101.
3 X. Wang, H. Fang, Z. Huang, W. Shang, T. Hou, A. Cheng and H. Cheng, *J. Mol. Med.*, 2013, **91**, 917–927.
4 B. B. Lahiri, S. Bagavathiappan, T. Jayakumar and J. Philip, *Infrared Phys. Technol.*, 2012, **55**, 221–235.
5 J. R. Casey, S. Grinstein and J. Orlowski, *Nat. Rev. Mol. Cell Biol.*, 2010, **11**, 50–61.
6 S. Endo, R. Kato, K. Sawada and T. Hattori, *Bull. Chem. Soc. Jpn.*, 2018, **91**, 304–310.
7 M. I. Khan, K. Mukherjee, R. Shoukat and H. Dong, *Microsyst. Technol.*, 2017, **23**, 4391–4404.

8 G. Miesenbock, D. De Angelis and J. Rothman, *Nature*, 1998, **394**, 192–195.
9 J. Whitaker, R. Haugland and F. Prendergast, *Anal. Biochem.*, 1991, **194**, 330–344.
10 S. Schlafer, J. E. Garcia, M. Greve, M. K. Raarup, B. Nyvad and I. Dige, *Appl. Environ. Microbiol.*, 2015, **81**, 1267–1273.
11 L. Zhang, F. Su, X. Kong, F. Lee, K. Day, W. Gao, M. E. Vecera, J. M. Sohr, S. Buizer and D. R. Meldrum, *RSC Adv.*, 2016, **6**, 46134–46142.
12 S. Schreml, R. J. Meier, K. T. Weiß, J. Cattani, D. Flittner, S. Gehmert, O. S. Wolfbeis, M. Landthaler and P. Babilas, *Exp. Dermatol.*, 2012, **21**, 951–953.
13 G. Ke, Z. Zhu, W. Wang, Y. Zou, Z. Guan, S. Jia, H. Zhang, X. Wu and C. J. Yang, *ACS Appl. Mater. Interfaces*, 2014, **6**, 15329–15334.
14 M. Anderson, A. Moshnikova, D. M. Engelman, Y. K. Reshetnyak and O. A. Andreev, *Proc. Natl. Acad. Sci.*, 2016, **113**, 8177–8181.
15 L. Ferrari, L. Rovati, P. Fabbri and F. Pilati, *Sensors*, 2013, **13**, 484–499.
16 G. S. Vasylevska, S. M. Borisov, C. Krause and O. S. Wolfbeis, *Chem. Mater.*, 2006, **18**, 4609–4616.
17 A. Kriltz, C. Loser, G. J. Mohr and S. Trupp, *J. Sol-Gel Sci. Technol.*, 2012, **63**, 23–29.
18 Y. Tian, F. Su, W. Weber, V. Nandakumar, B. R. Shumway, Y. Jin, X. Zhou, M. R. Holl, R. H. Johnson and D. R. Meldrum, *Biomaterials*, 2011, **31**, 7411–7422.
19 S. Schreml, R. J. Meier, O. S. Wolfbeis, M. Landthaler, R.-M. Szeimies and P. Babilas, *Proc. Natl. Acad. Sci.*, 2011, **108**, 2432–2437.
20 T. Fujie, *Polym. J.*, 2016, **48**, 773–780.
21 T. Miyagawa, T. Fujie, Ferdinandus, T. T. Vo Doan, H. Sato and S. Takeoka, *ACS Appl. Mater. Interfaces*, 2016, **8**, 33377–33385.
22 J. J. Richardson, M. Björnmalm and F. Caruso, *Science*, 2015, **348**, 2491–2501.
23 G. B. Monshausen, N. D. Miller, A. S. Murphy and S. Gilroy, *Plant J.*, 2011, **65**, 309–318.
24 M. a. Bacon, S. Wilkinson and W. J. Davies, *Plant Physiol.*, 1998, **118**, 1507–1515.
25 C. M. Geilfus, *Mol. Plant*, 2017, **10**, 1371–1386.
26 S. A. Smith and W. A. Pretorius, *Water SA*, 2002, **28**, 395–402.
27 T. Fujie, H. Haniuda and S. Takeoka, *J. Mater. Chem.*, 2011, **21**, 9112.
28 D. Yoo, S. S. Shiratori and M. F. Rubner, *Macromolecules*, 1998, **31**, 4309–4318.
29 W. S. Jang, A. T. Jensen and J. L. Lutkenhaus, *Macromolecules*, 2010, **43**, 9473–9479.
30 D. Wencel, T. Abel and C. McDonagh, *Anal. Chem.*, 2014, **86**, 15–29.
31 D. Aigner, S. M. Borisov, P. Petritsch and I. Klimant, *Chem. Commun.*, 2013, **49**, 2139–2141.
32 F. Wang, Y. Raval, H. Chen, T. R. J. Tzeng, J. D. Desjardins and J. N. Anker, *Adv. Healthcare Mater.*, 2014, **3**, 197–204.
33 H. H. Felle, *Plant Physiol.*, 1994, **106**, 1131–1136.
34 C. M. Geilfus and K. H. Mühling, *New Phytol.*, 2013, **197**, 1117–1129.
35 C. M. Geilfus and K. H. Mühling, *Plant Sci.*, 2014, **223**, 109–115.
36 C. M. Geilfus, A. Mithöfer, J. Ludwig-Müller, C. Zörb and K. H. Muehling, *New Phytol.*, 2015, **208**, 803–816.
37 T. Fujie, A. Saito, M. Kinoshita, H. Miyazaki, S. Ohtsubo, D. Saitoh and S. Takeoka, *Biomaterials*, 2010, **31**, 6269–6278.
38 K. Ito, A. Saito, T. Fujie, K. Nishiwaki, H. Miyazaki, M. Kinoshita, D. Saitoh, S. Ohtsubo and S. Takeoka, *Acta Biomater.*, 2015, **24**, 87–95.
39 J. S. Martinez, T. C. S. Keller and J. B. Schlenoff, *Biomacromolecules*, 2011, **12**, 4063–4070.
40 J. P. B. O'Connor, E. O. Aboagye and J. C. Waterton, *Nat. Rev. Clin. Oncol.*, 2017, **14**, 169–186.